SYNTHETIC BIOLOGY

Light-powered CO_2 fixation in a chloroplast mimic with natural and synthetic parts

Tarryn E. Miller[1], Thomas Beneyton[2], Thomas Schwander[1], Christoph Diehl[1], Mathias Girault[3], Richard McLean[1], Tanguy Chotel[2], Peter Claus[1], Niña Socorro Cortina[1], Jean-Christophe Baret[2,3]*, Tobias J. Erb[1,4]*

Nature integrates complex biosynthetic and energy-converting tasks within compartments such as chloroplasts and mitochondria. Chloroplasts convert light into chemical energy, driving carbon dioxide fixation. We used microfluidics to develop a chloroplast mimic by encapsulating and operating photosynthetic membranes in cell-sized droplets. These droplets can be energized by light to power enzymes or enzyme cascades and analyzed for their catalytic properties in multiplex and real time. We demonstrate how these microdroplets can be programmed and controlled by adjusting internal compositions and by using light as an external trigger. We showcase the capability of our platform by integrating the crotonyl–coenzyme A (CoA)/ethylmalonyl-CoA/hydroxybutyryl-CoA (CETCH) cycle, a synthetic network for carbon dioxide conversion, to create an artificial photosynthetic system that interfaces the natural and the synthetic biological worlds.

The photosynthetic transformation of inorganic carbon into organic matter is a fundamental biological process that is responsible for most of the stored energy and biomass on Earth. This process is spatially and temporally controlled and highly integrated with other cellular functions. Photosynthesis ultimately converts light energy through membrane-bound protein complexes into the energy-rich chemical cofactors adenosine triphosphate (ATP) and reduced nicotinamide adenine dinucleotide phosphate (NADPH). ATP and NADPH are subsequently used to fuel metabolic processes, particularly the fixation of CO_2 through the Calvin-Benson-Bassham cycle (*1*).

The principle of photosynthesis has been the inspiration for artificial systems that use the energy of light for the controlled capture and conversion of CO_2 into useful compounds (*2*–*9*). Two recent developments in bio- and nanotechnology promise to afford integrated systems of higher efficiency, approaching or rivaling that of natural biological systems. One is the emergence of microfluidics as a technology platform to manipulate and assemble constitutive elements and functions of living systems in miniaturized and confined environments (*4*, *10*–*16*). The second is the successful design and realization of complex biomimetic modules and systems from defined biological parts. Recent examples are metabolically active microcompartments, artificial light-harvesting organelles (*17*–*20*), advanced transcription-translation circuits (*21*, *22*), and complex, in vitro metabolic networks (*23*–*25*). However, the combination of these individual modules into more complex systems remains a challenge (*26*). Here, we developed a platform for the automated assembly of picoliter-sized reaction compartments that enable the light-driven conversion of CO_2 into multicarbon compounds (i.e., glycolate), mimicking the function of chloroplasts.

In photosynthesis, thylakoid membranes provide the energy for CO_2 fixation, and we sought to exploit this ability directly for biocatalytic and synthetic biological applications. To establish a module for the light-driven regeneration of ATP and NADPH, we isolated thylakoid membranes from the chloroplasts of *Spinacia oleracea*. At 100 μmol photons m^{-2} s^{-1}, these thylakoid preparations catalyzed the light-dependent reduction of $NADP^+$ to NADPH (with concomitant oxygen evolution) at a specific activity of 3.41 ± 0.01 μmol min^{-1} μg^{-1} total chlorophyll (Chl, sum of Chl A and B; Fig. 1A), which is comparable to values measured by others (table S1). NADPH regeneration required the addition of external ferredoxin, with an optimum concentration of 5 μM (figs. S1A and S1B). Supply of external ferredoxin:$NADP^+$ reductase (FNR) did not increase activity further (fig. S6A). Addition of superoxide dismutase and catalase to scavenge reactive oxygen species (ROS) resulted in prolonged thylakoid membrane activity (fig. S2D). In the following experiments, we used light intensities between 50 and 60 μmol photons m^{-2} s^{-1} to further minimize the formation of ROS, which would damage the photosynthetic apparatus (e.g., the D1 subunit), while providing sufficient rates of NADPH regeneration (fig. S2E).

Thylakoid membranes also catalyzed the regeneration of ATP from adenosine diphosphate (ADP) both in the light and in the dark. ATP regeneration in the dark was quantified at 1.2 ± 0.2 μM min^{-1} μg^{-1} Chl, attributed to membrane-bound adenylate kinases (*27*), which could be suppressed by using an adenylate kinase–specific inhibitor, diadenosine pentaphosphate (DAPP) (*28*, *29*) (fig. S1C). In the light, ATP production from ADP increased sixfold (6.5 ± 0.5 mM min^{-1} mg^{-1} Chl). Addition of DAPP resulted in a light- (and ATPase-) dependent ATP synthesis rate of 5.4 ± 0.5 mM min^{-1} mg^{-1} Chl (Fig. 1B), comparable to previous studies. The specific activities of thylakoid membranes varied slightly between individual preparations (fig. S1E). Thylakoid membranes were stably maintained in the dark for at least 2 hours at room temperature and for at least 24 hours when maintained on ice, with no observable loss of NADPH productivity upon illumination (fig. S1D). Membrane preparations could be stored at −80°C for >1 year without notable loss of activity (fig. S1E), demonstrating their usability as a thylakoid membrane–based energy module (TEM).

Next, we tested the ability of TEM to energize individual enzyme reactions. We coupled the TEM with two different CO_2-fixing enzymes, crotonyl-coenzyme A (CoA) carboxylase/reductase (Ccr) and propionyl-CoA carboxylase (Pcc), which require NADPH and ATP, respectively (Fig. 1C). In the case of Ccr, product formation was strictly light dependent with a CO_2-fixation rate of 5.2 ± 0.2 μM min^{-1} μg^{-1} Chl (Fig. 1D). Pcc showed a light-dependent CO_2-fixation rate of 5.1 ± 0.2 μM min^{-1} μg^{-1} Chl (Fig. 1D) and a low, light-independent carboxylation rate of 0.8± 0.1 μM min^{-1} μg^{-1} Chl, which was caused by the adenylate kinase activity of the TEM (see above). These carboxylation rates are more than three orders of magnitude higher than recent efforts to couple enzymatic CO_2 fixation to isolated photosystem II (PSII) (~6.9×10^4 molecules h^{-1} per PSII reaction center compared with 34 molecules h^{-1} per PSII reaction center; table S2), highlighting the capability of our TEM to energize catalytic transformations.

We sought to test the capacity of the TEM to not only power individual CO_2-fixing reactions, but a complete metabolic cycle for the continuous fixation of CO_2. To that end, we combined the 16 enzymes of the crotonyl-CoA/ethylmalonyl-CoA/hydroxybutyryl-CoA (CETCH) cycle (version 5.4) (*23*), an artificial pathway for the fixation of CO_2 in vitro, and a glyoxylate/hydroxypyruvate reductase from *Escherichia coli* (Ghr) with the TEM (Fig. 2A). Initial efforts to operate the CETCH cycle together with the TEM failed, indicating a negative interaction of system components (fig. S3). One problem was an intrinsic hydratase activity of TEM converting crotonyl-CoA into

[1]Department of Biochemistry and Synthetic Metabolism, Max Planck Institute for Terrestrial Microbiology, D-35043 Marburg, Germany. [2]University of Bordeaux, CNRS, Centre de Recherche Paul Pascal, UMR 5031, Pessac 33600, France. [3]Institut Universitaire de France, Paris 75005, France. [4]Center for Synthetic Microbiology, Max Planck Institute for Terrestrial Microbiology, D-35043 Marburg, Germany.
*Corresponding author. Email: toerb@mpi-marburg.mpg.de (T.J.E.); jean-christophe.baret@u-bordeaux.fr (J.-C.B.)

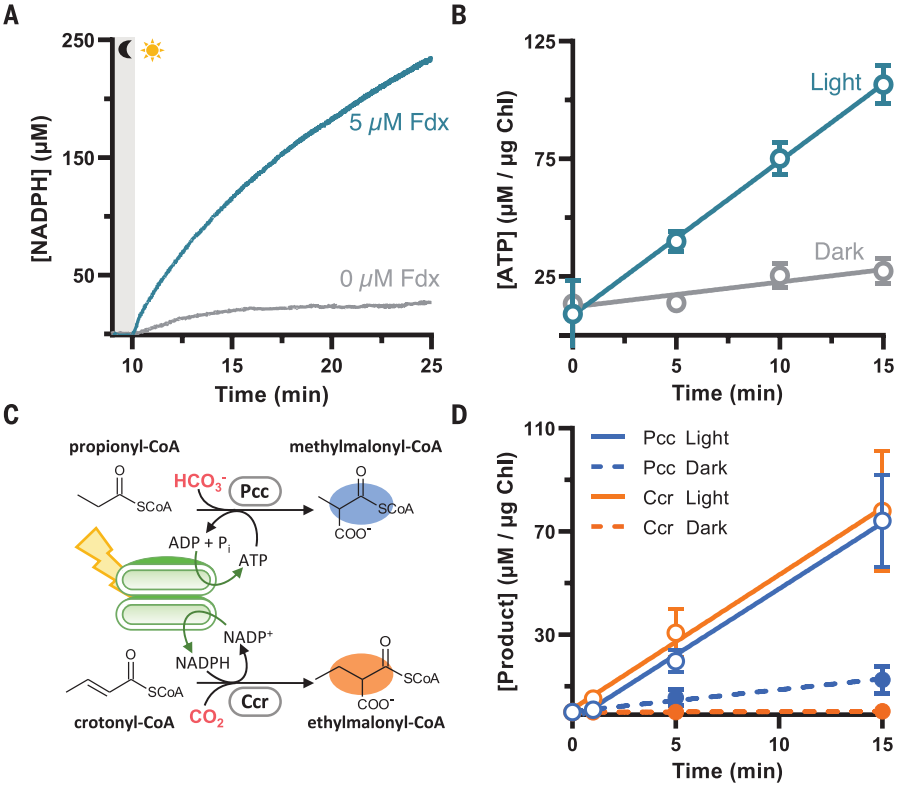

Fig. 1. Light-driven cofactor regeneration by TEM. (**A**) NADPH production is dependent on light and externally added ferredoxin. (**B**) ATP production is dependent on light, with some background reaction in the dark caused by membrane-bound adenylate kinase (fig. S1C). (**C**) Scheme of TEM-driven carboxylation reactions of Pcc and Ccr using light-produced ATP and NADPH, respectively. (**D**) Reactions coupled to TEM (2.5 or 5 μg Chl and 60 μmol photons m^{-2} s^{-1}) (N = 6).

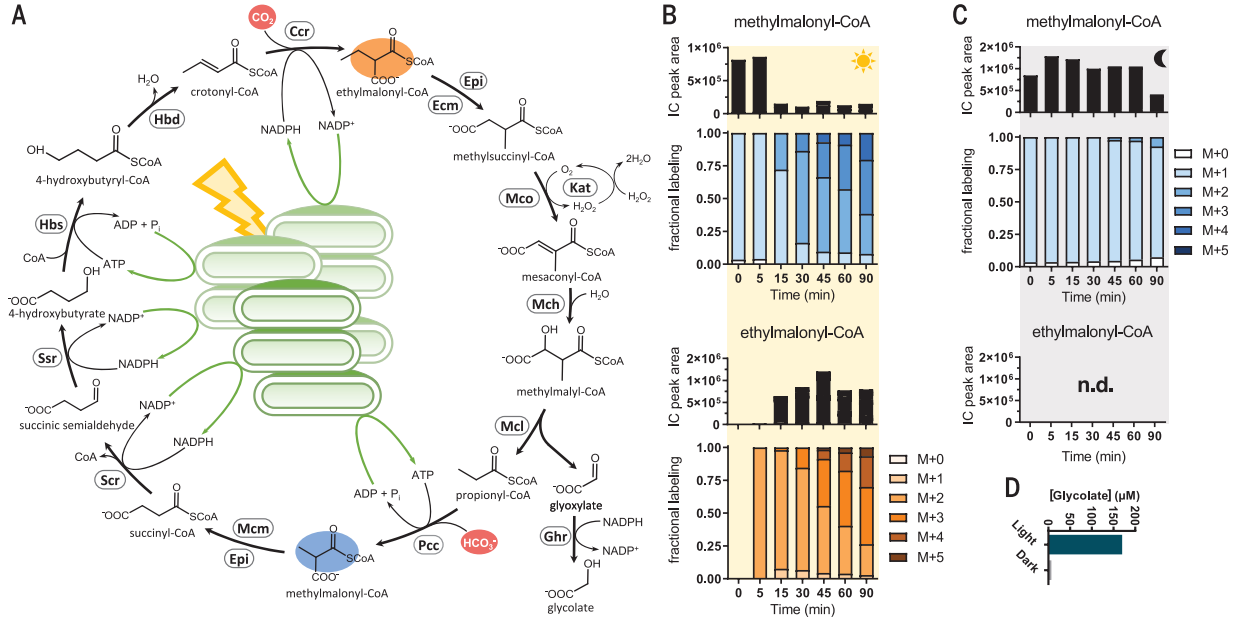

Fig. 2. Light-driven, continuous fixation of CO_2 into organic acids. (**A**) Scheme of CETCH version 6.0 for the conversion of CO_2 into glycolate coupled to TEM. (**B** and **C**) ^{13}C-labeling patterns and total levels of methylmalonyl-CoA (blue) and ethylmalonyl-CoA (orange) over time, starting the CETCH cycle with 80 μM propionyl-CoA. (B) CETCH cycle version 6.0 directly operated by 125 μg Chl ml^{-1} TEM under constant illumination (60 μmol photons m^{-2} s^{-1}). Shown is the extracted ion peak area and the fractional labeling of ethylmalonyl-CoA, as well as methylmalonyl-CoA (in shades of orange and blue, respectively; see fig. S4 for an explanation of the labeling pattern). IC, ion count. (C) Same as (B) but in the dark, showing that light is required to operate the cycle. Ethylmalonyl-CoA is not produced in the dark when starting from propionyl-CoA. n.d., not detected. (**D**) Glycolate production in the light and the dark by CETCH version 6.0.

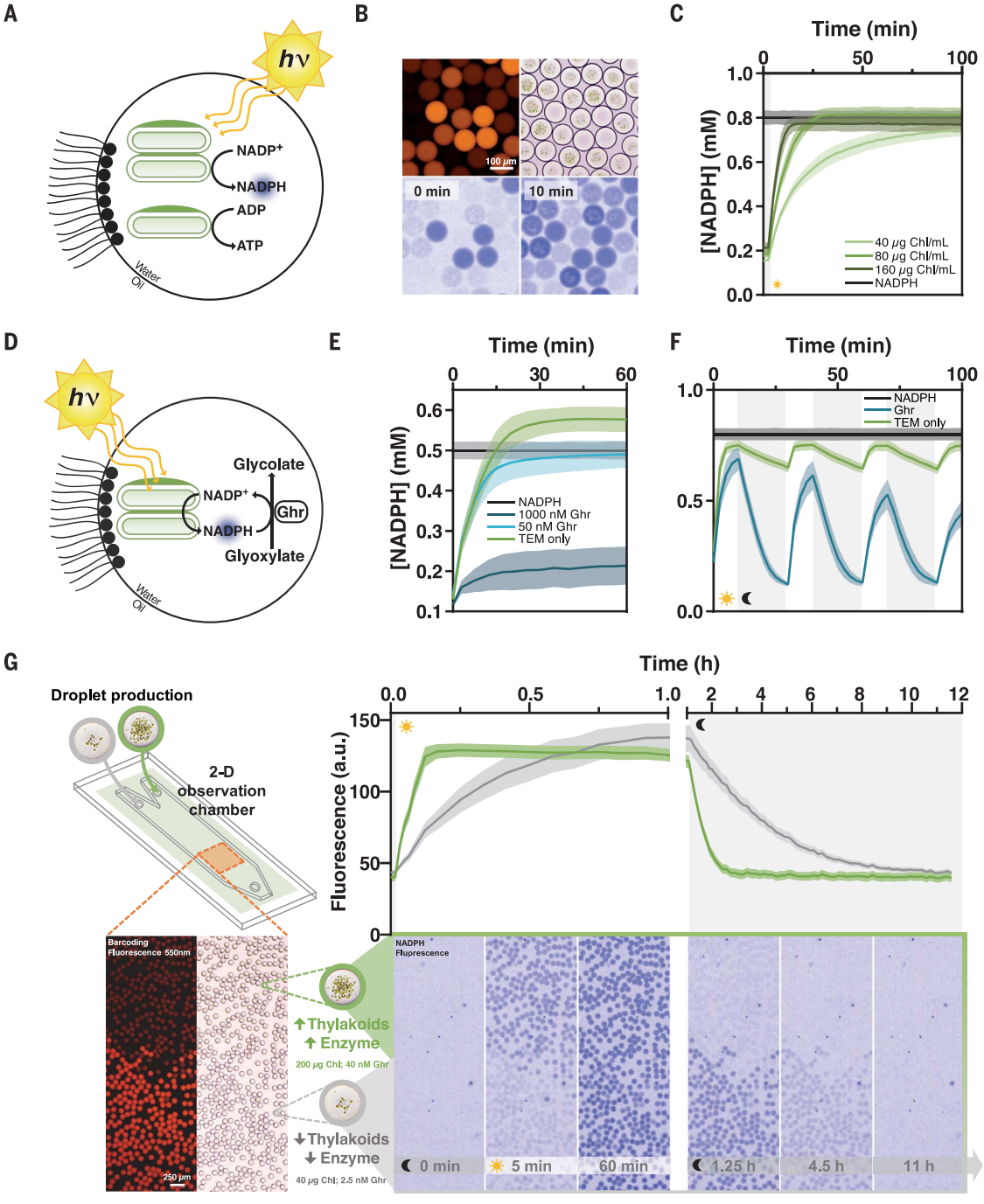

Fig. 3. Encapsulation of a functional TEM in microdroplets and light-driven enzymatic reaction coupled to TEM in microdroplets. (**A**) Scheme of the TEM system encapsulated in microdroplets. Light triggers TEM activity to produce NADPH and ATP. NADPH production is monitored by NADPH fluorescence (365 nm) of individual droplets. Populations of droplets can be distinguished from one another through the addition of a bar-coding dye. hν, photon energy. (**B**) Microscopic photographs of a representative four-bit emulsion of droplets containing four different TEM concentrations. First row, left to right: barcoding fluorescence, bright field. Second row, left to right: NADPH fluorescence at time point 0 and NADPH fluorescence after 10 min of illumination. A time-lapse video of the increasing NADPH fluorescence is available as movie S1. (**C**) NADPH concentration versus time of microdroplets with varying TEM. (**D**) Scheme of the TEM-powered reduction of glyoxylate into glycolate by Ghr encapsulated in microdroplets. (**E**) TEM-driven conversion (65 μg Chl ml^{-1}) of glyoxylate (5 mM) by Ghr in microdroplets (N = 50). The concentration of Ghr changes the steady-state level of NADPH at 50 μmol photons m^{-2} s^{-1}. (**F**) TEM-driven conversion of glyoxylate (120 μg Chl ml^{-1} and 5 mM, respectively) in microdroplets under programmed light-dark cycles. Shown is the photoreduction of $NADP^+$ in droplets (N = 50) with 53.5 nM Ghr (teal line) under alternating cycles of illumination (50 μmol photons m^{-2} s^{-1}) and darkness. Control: Droplets containing no Ghr (green line) and droplets containing 1 mM NADPH (black line). A time-lapse video of oscillations is available as movie S2. In (C), (E), and (F), bold lines indicate the mean of the droplet population. Shaded areas indicate ± SD (N = 50). (**G**) Time and space control of metabolic activity in droplets. A binary emulsion of droplets with two different TEM and Ghr concentrations was created. A spatial pattern was created by filling the droplets into an observation chamber, with each population filling approximately half of the chamber. The plot shows relative NADPH fluorescence over time under fluctuating light conditions (dark, 50 μmol photons m^{-2} s^{-1}) for both droplet populations, with the same color coding. A time-lapse video of NADPH fluorescence is available as movie S3.

3-hydroxybutyryl-CoA (fig. S5), which we addressed by the addition of a crotonase from *Pseudomonas aeruginosa* (PhaJ) (*30*) for metabolite proofreading (*31*). Further analysis suggested that the flavin adenine dinucleotide (FAD)–dependent enzymes methylsuccinyl-CoA oxidase (Mco) and propionyl-CoA oxidase (Pco) interfered with TEM productivity, likely because of the formation of ROS and free FAD in the enzyme preparation (fig. S6). The latter is capable of directly oxidizing NADPH through the interaction with FNR (see also figs. S3, A and B, and S6, B and C). When we replaced Pco with Pcc and added Ghr as an output module (creating CETCH

cycle version 6.0; Fig. 2, A to C), the coupled system produced 156 μM glycolate from 120 μM acceptor molecule (Fig. 2D). Replacing Mco with a methylsuccinyl-CoA dehydrogenase (Mcd), its cognate electron transfer protein (Etf), as well as an Etf-ubiquinone oxidoreductase (creating CETCH cycle version 7.0), further improved glycolate formation from CO_2 and light (fig. S7).

The above results demonstrated that the synthetic CETCH cycle can be functionally coupled to the native energy machinery of photosynthesis in a fully integrated fashion using light energy to form multicarbon compounds from CO_2. Realizing the limitations of individual bulk experiments (e.g., sample volume, self-shading effects, number of parallel assays, and no real-time monitoring), we further envisioned to miniaturize our experimental setup for parallelization, multiplexing, and high-throughput analysis. We therefore developed a droplet-based microfluidic platform for the automated assembly of metabolically active microcompartments that can be controlled and powered by external illumination and analyzed in real time (fig. S8).

In a first step, we encapsulated the TEM into water-in-oil microdroplets (300 pl; 92 μm in diameter; Fig. 3, A and B) and studied their metabolic activity by assessing NADPH fluorescence in single droplets using microscopy (figs. S8 and S9). Encapsulating thylakoid membranes produced droplets with a specifically defined number of TEM granules (~100) with a maximum droplet-to-droplet variation of 20%, which is expected from a random encapsulation process (fig. S10B). We further used orthogonal fluorescent bar coding to multiplex different populations of droplets (*10*), which allowed us to quantify the local chemical and metabolic states of hundreds of individual droplets of different composition in one experiment in parallel.

We then used multiplexing to study and optimize the activity of droplet-encapsulated TEM granules. $NADP^+$ photoreduction in droplets was strictly dependent on illumination and directly correlated to the number of TEM granules, following a correlation with chlorophyll content (Fig. 3C and fig. S11). We observed a maximum photoreduction rate of 2.0 ± 0.1 (95% confidence interval) NADPH μmol min^{-1} μg^{-1} Chl at 50 μmol photons m^{-2} s^{-1}, which is comparable to rates obtained earlier in bulk experiments. Droplet-to-droplet variation in NADPH production was largely determined by statistical fluctuations of the number of encapsulated TEM granules (fig. S10C). We further characterized and optimized the operating conditions of the TEM in microdroplets. Sorbitol at 700 mM increased the stability of the TEM by several hours (fig. S11). $NADP^+$ photoreduction increased with higher light intensities from 50 to 200 μmol photons m^{-2} s^{-1}, above which NADPH production rates decreased again, likely because of photodamage of the TEM (fig. S12). $NADP^+$ photoreduction was operable and stable over light-dark cycles (figs. S13, S14D, and S15B), demonstrating that the TEM could be switched on and off in individual droplets.

We next tested the capability of TEM-containing droplets to power individual enzyme reactions by coencapsulation of enzymes and substrates. First, we tested Ghr, which catalyzes the NADPH-dependent reduction of glyoxylate to glycolate (Fig. 3D). At 120 μg Chl ml^{-1} reaction mixture, 8.2 μg ml^{-1} Ghr, and 50 μmol photons m^{-2} s^{-1}, we observed production of 4.7 mM glycolate (starting from 5 mM glyoxylate and only 0.8 mM $NADP^+$) after 75 min in the light and no production in

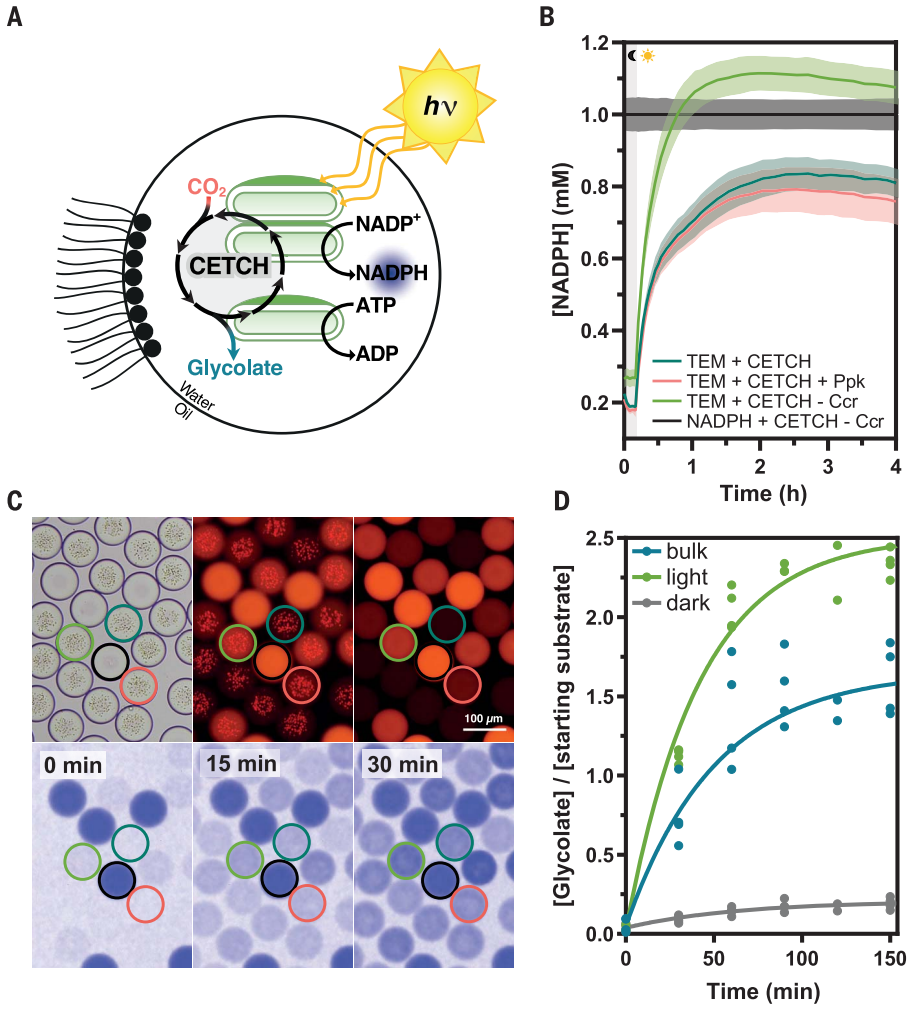

Fig. 4. Light-driven, continuous fixation of CO_2 into organic acids by CETCH version 7.0 coupled to TEM in microdroplets. (**A**) Scheme of the CETCH version 7.0 coupled to TEM operating inside microdroplets. (**B**) Dynamic equilibrium states of NADPH fluorescence of four populations of droplets: (i) Droplets containing TEM (60 μg Chl ml^{-1}), 1 mM $NADP^+$, and CETCH version 7.0 (teal line); (ii) droplets containing TEM, 1 mM $NADP^+$, and an additional ATP regeneration system [polyphosphate kinase (Ppk) and polyphosphate, coral line]; (iii) control droplets containing 1 mM NADPH and all CETCH version 7.0 components except for Ccr (black line); and (iv) control droplets containing TEM, 1 mM $NADP^+$, and all CETCH version 7.0 components except for Ccr (green line). (**C**) Images of the droplets from (B) using the same color coding; first row, left to the right: bright field, thylakoid fluorescence with overlap from the coding dye, and coding dye; second row, left to the right: NADPH fluorescence before illumination, after 15 min of illumination, and after 30 min of illumination. A time-lapse video is available as movie S4. (**D**) Glycolate formed per acceptor molecule (sum of crotonyl-CoA and 3-hydroxybutyryl-CoA) over time in droplets and in bulk solution. The light and dark curves represent droplets maintained in the light and in the dark, respectively. The bulk curve shows an experiment with the same reaction mixture but on the microtube scale, kept in the dark for the duration of droplet manufacture. The bulk solution and the droplets were simultaneously exposed to light for parallel comparison.

the dark control. Varying the number of TEM granules and the concentrations of substrate and Ghr in individual droplet populations resulted in distinct dynamic NADPH equilibrium states (Fig. 3, D to F, and fig. S14), reflecting the real-time cofactor production and consumption rates in the different populations of droplets. Light-dark cycles could be used to temporally regulate cofactor regeneration and enzyme kinetics in droplet populations (Fig. 3F).

The homogeneous behavior of droplet populations enabled us to subsequently program the metabolic activity of reaction compartments in a predictable fashion. To demonstrate this, we created a patterned emulsion of two populations of droplets differing in TEM and Ghr concentration. This binary emulsion was activated by illumination, resulting in distinct NADPH production rates, depending on the TEM concentration in the two droplet populations. In a subsequent dark phase, NADPH was consumed at distinct rates that were correlated to different Ghr loading of the two populations (Fig. 3G and movie S3), demonstrating the high level of spatial, temporal, and synchronized control over individual reaction compartments that can be achieved with our platform. Similar results were also obtained for other droplet-encapsulated enzymes that required ATP and/or NADPH, namely propionyl-CoA synthase (Pcs) and Ccr (figs. S15 and S16). Using Ccr, we measured single-enzyme CO_2-fixation rates of 6.4 μmol min^{-1} mg^{-1} Chl in droplets. Without any further optimization, these rates are more than two orders of magnitude higher than recent reports of coupling PSII reaction centers to pyruvate carboxylase (*18*), comparable to values reached for PSII-coupled photoelectrochemical hydrogen production [notably, without CO_2 fixation (*5*)] and reaching levels measured for isolated chloroplasts (table S2).

Having created photosynthetic microcompartments powering single-enzyme reactions, we ultimately aimed at encapsulating and screening different variants of the CETCH cycle inside TEM-containing droplets (Fig. 4). After further optimizing the preparation of droplets for enzymes and metabolites of the CETCH cycle (fig. S17), we encapsulated different CETCH cycle versions together with TEM and monitored the dynamic equilibrium state of NADPH. This allowed us to directly quantify the behavior of different CETCH variants in hundreds of microcompartments side by side and in real time, which would not have been possible in bulk experiments (Fig. 4, B and C, and fig. S18, A and B). Droplets with CETCH based on Mcd (version 7.0) maintained TEM activity longer than droplets containing CETCH based on Mco (version 6.0) (fig. S18). Supply of an additional ATP regeneration module (Ppk and polyphosphate) did not increase activity further (Fig. 4, B and C), suggesting that cofactor regeneration was not limiting productivity of our integrated photosynthetic system, but rather the concentration, intrinsic properties, and/or interplay of the individual components of our system, such as the stability of CoA-thioester intermediates (fig. S17). Without further optimization, our integrated system was able to produce 47 ± 5 μM glycolate from CO_2 over 90 min in droplets (Fig. 4D). Thus, although the overall productivity of our complex system was lower compared with Ccr alone, it still outperforms other efforts using only single enzymes (*18*). For the full CETCH cycle, we calculated a carbon-conversion efficiency of ~3.5% in our microcompartments (NADPH consumption rate of CO_2 reduction divided by the measured maximum rate of $NADP^+$ photoreduction achieved in droplets). Overall, our results demonstrated that it is possible to interface natural and synthetic biological modules in thousands of cell-sized compartments to create new-to-nature photosynthetic entities that have the potential to outcompete natural photosynthesis (i.e., because of a more efficient CO_2-fixation metabolism that does not suffer from photorespiration).

The technical capability to reconstruct, control, and study complex reaction networks in a cell-like environment will be of use for both top-down and bottom-up synthetic biology. Prototyping complex metabolic reaction cascades in miniaturized compartments has the potential to provide new means for metabolic engineering. Technical advancements, especially the development of combinatorial screening methods (*32*) and bar-coding techniques to encode reaction conditions in microfluidics-based high-throughput screening (*33*) could further enhance multiplexing capabilities and guide future efforts of testing and optimizing the CETCH cycle and other new-to-nature pathways before their transplantation into living cells.

Our efforts also demonstrate how natural and synthetic biological modules can be mixed and matched to create highly integrated systems that show lifelike functions. Our "synthetic chloroplast" has the essential characteristics of photosynthesis that allow the formation of biological building blocks from inorganic carbon, providing the basis to develop a self-sustained, completely synthetic "designer" carbon metabolism in our artificial organelle. Future implementation of other life characteristics such as self-repair and reproduction, as well as information processing and regulatory circuits, will further contribute to the realization of synthetic organelles and cells from the bottom up that approach—or may even exceed—a grade of organization, integration, and functional efficiency comparable to their natural counterparts (*4*).

REFERENCES AND NOTES

1. J. A. Bassham, A. A. Benson, M. Calvin, *J. Biol. Chem.* **185**, 781–787 (1950).
2. C. Liu, B. C. Colón, M. Ziesack, P. A. Silver, D. G. Nocera, *Science* **352**, 1210–1213 (2016).
3. K. Jensen, P. E. Jensen, B. L. Møller, *Trends Plant Sci.* **17**, 60–63 (2012).
4. P. Schwille *et al*., *Angew. Chem. Int. Ed. Engl.* **57**, 13382–13392 (2018).
5. K. P. Sokol *et al*., *Nat. Energy* **3**, 944–951 (2018).
6. J. Guo *et al*., *Science* **362**, 813–816 (2018).
7. K. K. Sakimoto, A. B. Wong, P. Yang, *Science* **351**, 74–77 (2016).
8. W. Zhang *et al*., *Nat. Catal.* **1**, 55–62 (2018).
9. Z. C. Litman, Y. Wang, H. Zhao, J. F. Hartwig, *Nature* **560**, 355–359 (2018).
10. T. Beneyton *et al*., *Nat. Commun.* **9**, 2391 (2018).
11. M. Weiss *et al*., *Nat. Mater.* **17**, 89–96 (2018).
12. S. Deshpande *et al*., *Nat. Commun.* **10**, 1800 (2019).
13. K. Hasatani *et al*., *Chem. Commun.* **49**, 8090–8092 (2013).
14. A. Dupin, F. C. Simmel, *Nat. Chem.* **11**, 32–39 (2019).
15. M. J. Booth, V. Restrepo Schild, S. J. Box, H. Bayley, *Sci. Rep.* **7**, 9315 (2017).
16. R. Booth, Y. Qiao, M. Li, S. Mann, *Angew. Chem. Int. Ed. Engl.* **58**, 9120–9124 (2019).
17. S. Berhanu, T. Ueda, Y. Kuruma, *Nat. Commun.* **10**, 1325 (2019).
18. K. Y. Lee *et al*., *Nat. Biotechnol.* **36**, 530–535 (2018).
19. X. Feng, Y. Jia, P. Cai, J. Fei, J. Li, *ACS Nano* **10**, 556–561 (2016).
20. B. C. Buddingh', J. C. M. van Hest, *Acc. Chem. Res.* **50**, 769–777 (2017).
21. A. M. Tayar, E. Karzbrun, V. Noireaux, R. H. Bar-Ziv, *Proc. Natl. Acad. Sci. U.S.A.* **114**, 11609–11614 (2017).
22. M. Yelleswarapu *et al*., *ACS Synth. Biol.* **7**, 2879–2887 (2018).
23. T. Schwander, L. Schada von Borzyskowski, S. Burgener, N. S. Cortina, T. J. Erb, *Science* **354**, 900–904 (2016).
24. N. Srinivas, J. Parkin, G. Seelig, E. Winfree, D. Soloveichik, *Science* **358**, eaal2052 (2017).
25. Q. M. Dudley, A. S. Karim, M. C. Jewett, *Biotechnol. J.* **10**, 69–82 (2015).
26. M. J. Booth, V. Restrepo Schild, F. G. Downs, H. Bayley, *Mol. Biosyst.* **13**, 1658–1691 (2017).
27. S. Murakami, H. Strotmann, *Arch. Biochem. Biophys.* **185**, 30–38 (1978).
28. D. D. Strand, N. Fisher, D. M. Kramer, *J. Biol. Chem.* **292**, 11850–11860 (2017).
29. G. E. Lienhard, I. I. Secemski, *J. Biol. Chem.* **248**, 1121–1123 (1973).
30. T. Fukui, N. Shiomi, Y. Doi, *J. Bacteriol.* **180**, 667–673 (1998).
31. J. Sun, J. G. Jeffryes, C. S. Henry, S. D. Bruner, A. D. Hanson, *Metab. Eng.* **44**, 150–159 (2017).
32. A. Kulesa, J. Kehe, J. E. Hurtado, P. Tawde, P. C. Blainey, *Proc. Natl. Acad. Sci. U.S.A.* **115**, 6685–6690 (2018).
33. C. M. Svensson *et al*., *Small* **15**, e1802384 (2019).
34. T. E. Miller *et al*., Data and computational codes for: Light-powered CO_2 fixation in a chloroplast mimic with natural and synthetic parts, Zenodo (2020); https://doi.org/10.5281/zenodo.3724502.

ACKNOWLEDGMENTS

We thank J. Zarzycki, D. Strand, and S. Burgener for enlightening discussions and G. Stoffel for providing CoA esters. **Funding:** This work was supported by the Max Planck Society (MaxSynBio), the European Research Council (grant no. ERC 637675 "SYBORG"), and the U.S. Department of Energy Joint Genome Institute, a DOE Office of Science User Facility (contract no. DE-AC02-05CH11231) with T.J.E. as grantee. J.-C.B. acknowledges financial support by the Region Nouvelle Aquitaine and by the French Government's Investments for the Future Programme, University of Bordeaux Initiative of Excellence (IDEX Bordeaux; (ANR)-10-IDEX-03-02). T.E.M. and R.M. were supported by the International Max Planck Research School for Environmental, Cellular and Molecular Microbiology (Marburg, Germany). **Author contributions:** The project was conceived by T.E.M., T.B., T.S., J.-C.B., and T.J.E. Characterization and optimization of thylakoid preparations was done by T.E.M. Couplings of the CETCH cycle to thylakoids in bulk were performed by T.E.M. together with T.S. and C.D. The ETF:QO system as electron acceptor for Etf was developed by T.E.M and R.M. Mass spectrometric analyses were performed by N.C.S. and P.C., and these data were analyzed by T.E.M. The microfluidic

platform to encapsulate thylakoids was developed by T.B. and J.-C.B. Microfluidic experiments were planned, performed, and analyzed by T.B. and T.E.M. with assistance from T.C. The software for light-dark cycles time-lapse fluorescence microscopy, as well as the image-processing software to analyze TEM activity in droplets, was developed by M.G. Experimental data were analyzed by T.E.M., T.B., and T.J.E. The manuscript was written by T.E.M., T.B., J.-C.B., and T.J.E. with contributions from all other authors. **Competing interests:** J.-C.B. is a founder and scientific adviser at Emulseo. The authors declare no other competing interests. **Data and materials availability:** All data are available in the main text or supplemental materials. The LabVIEW code used for image analysis has been deposited to GitHub (*34*).

SUPPLEMENTARY MATERIALS

science.sciencemag.org/content/368/6491/649/suppl/DC1
Materials and Methods
Figs. S1 to S18
Tables S1 to S9
References (*35*–*64*)
Movies S1 to S4

View/request a protocol for this paper from *Bio-protocol*.

30 September 2019; accepted 24 March 2020
10.1126/science.aaz6802

Science

Light-powered CO_2 fixation in a chloroplast mimic with natural and synthetic parts

Tarryn E. Miller, Thomas Beneyton, Thomas Schwander, Christoph Diehl, Mathias Girault, Richard McLean, Tanguy Chotel, Peter Claus, Niña Socorro Cortina, Jean-Christophe Baret and Tobias J. Erb

Science **368** (6491), 649-654.
DOI: 10.1126/science.aaz6802

Hybrid approach catches light

Plant chloroplasts enclose two major photosynthetic processes: light reactions, which generate the energy carriers adenosine triphosphate and reduced nicotinamide dinucleotide phosphate (NADPH), and dark reactions, which use these molecules to fix carbon dioxide and build biomass. Miller *et al.* appropriated natural components, thylakoid membranes from spinach, for the light reactions and showed that these could be coupled to a synthetic enzymatic cycle that fixes carbon dioxide within water-in-oil droplets. The composition of the droplets could be tuned and optimized and the metabolic activity monitored in real time by NADPH fluorescence (see the Perspective by Gaut and Adamala). These chloroplast-mimicking droplets bring together natural and synthetic components in a small space and are amenable to further functionalization to perform complex biosynthetic tasks.

Science, this issue p. 649; see also p. 587

Science (print ISSN 0036-8075; online ISSN 1095-9203) is published by the American Association for the Advancement of Science, 1200 New York Avenue NW, Washington, DC 20005. The title *Science* is a registered trademark of AAAS.